DRAFT-IDETC2020-11300

SAND2020-3664C

WearGP: A UQ/ML wear prediction framework for slurry pump impellers and casings

Anh Tran*
Optimization and Uncertainty Quantification
Sandia National Laboratories
Albuquerque, NM 87123
Email: anhtran@sandia.gov

Yan Wang
Woodruff School of Mechanical Engineering
Georgia Institute of Technology,
Atlanta, GA 30332
Email: yan.wang@me.gatech.edu

John Furlan
GIW Industries, Inc.
Grovetown, GA 30830
Email: John.Furlan@ksb.com

Krishnan V. Pagalthivarthi
GIW Industries, Inc.
Grovetown, GA 30830
Email: cfdconsult@outlook.com

Mohamed Garman
GIW Industries, Inc.
Grovetown, GA 30830
Email: Mohamed.Garman@ksb.com

Aaron Cutright
GIW Industries, Inc.
Grovetown, GA 30830
Email: Aaron.Cutright@ksb.com

Robert Visintainer
GIW Industries, Inc.
Grovetown, GA 30830
Email: Robert.Visintainer@ksb.com

– Dedicated to the memory of John Furlan.

Wear prediction is important in designing reliable machinery for slurry industry. It usually relies on multi-phase computational fluid dynamics, which is accurate but computationally expensive. Each run of the simulations can take hours or days even on a high-performance computing platform. The high computational cost prohibits a large number of simulations in the process of design optimization. In contrast to physics-

*Corresponding author: anhtran@sandia.gov, also affiliated with GIW Industries, Inc.

Sandia National Laboratories is a multimission laboratory managed and operated by National Technology & Engineering Solutions of Sandia, LLC, a wholly owned subsidiary of Honeywell International Inc., for the U.S. Department of Energy's National Nuclear Security Administration under contract DE-NA0003525.

based simulations, data-driven approaches such as machine learning are capable of providing accurate wear predictions at a small fraction of computational costs, if the models are trained properly. In this paper, a recently developed WearGP framework [1] is extended to predict the global wear quantities of interest by constructing Gaussian process surrogates. The effects of different operating conditions are investigated. The advantages of the WearGP framework are demonstrated by its high accuracy and low computational cost in predicting wear rates.

Nomenclature

BO Bayesian optimization
CFD computational fluid dynamics
DL deep learning
GP Gaussian process
HPC high-performance computer/computing
ML machine learning
NN neural networks
UQ uncertainty quantification
QoI(s) quantity/quantities of interests

1 Introduction

Accurate wear predictions and estimation of total cost of ownership for centrifugal pumps are critical for the slurry industry [2]. Pump failures can occur due to wears in various components, such as impellers, casings, and liners. Unplanned shutdowns in customers' production lines caused by component failures can be extremely expensive. To improve the quality, multi-phase computational fluid dynamics (CFD) is typically applied to predict slurry erosion of different pump components during design, for example, pump impeller [3] and pump casing [4,5] degradation. However, CFD simulations are computationally expensive. Repetitively running simulations during design optimization is not affordable under the time constraint of product development. Instead of relying on physics-based simulations, utilizing data-driven models such as machine learning (ML) techniques for wear prediction can significantly reduce the computational cost while maintaining prediction accuracy, if the models are trained properly. Its low computational cost also allows one to efficiently explore the high-dimensional design space, if the ML models are sufficiently calibrated. Recently, a WearGP framework [1] was developed to predict wear rates based on Gaussian process surrogate models. In this paper, the framework is extended to predict the global quantities of interests (QoIs). The QoIs under different pump operating conditions are explored.

ML approaches for simulation predictions recently attracted much research attention. Black-box or data-driven approaches such as neural networks (NNs) and deep learning (DL) are among the most popular techniques used for predicting simulation outcome. For example, Chang et al. [6] proposed a DL-based slip model constraining momentum and internal energy equations to simulate a boiling water reactor channel ranging from subcool liquid to a boiling flow. Zhu et al. [7] proposed a convolutional encoder-decoder framework to incorporate the governing equations of the physical models into the loss function, and trained the DL architecture without computing the solution of the partial differential equations, which can be considered as a significant advance, because one of the most considerable bottlenecks in training DL models to attain high accuracy is the need for a large amount of data, which is a resource-intensive process. As a gray-box approach, Liu and Wang [8] developed a multi-fidelity physics-constrained neural network architecture, which can be trained based on only a small amount of simulation data, to predict solutions of partial differential equations. Xiao et al. [9, 10, 11, 12] proposed a data-driven approach to predict the discrepancy of Reynolds-stress tensors based on direct numerical simulation datasets and correct the Reynolds-average Navier-Stokes predictions. Regarding wear and tribological applications, Friedrich et al. [13, 14] and Suresh et al. [15] employed NNs to predict experimental wear for polymers. Danaher et al. [16] also utilized NNs to predict erosion wear in Ni-base alloys at high temperature. Shamshirband et al. [17] developed a NN architecture to predict erosion wear in a 90° elbow, trained by CFD simulations, where the QoIs (total erosion and maximum erosion rate) are global variables. Pandya et al. [18] employed NNs to predict erosion wear using ANSYS Fluent as a training CFD model. Different from the above, Qu and Zuo [19] utilized support vector machines as a classification tool to determine the degree of wear for slurry pump impellers. Dai et al. [20] employed a Gaussian process (GP) framework to quantify uncertainty in predicting erosive wear after mining data.

In our previous work, a GP-based machine learning framework, called WearGP [1], is developed to predict CFD wear results locally given mesh and wear datasets. Our approach has demonstrated the efficiency of GP in small data regime, where there is insufficient data to train a deep learning model (only 144 simulations are used as the training dataset). In this paper, the WearGP framework is extended to predict the wear rates as global QoIs for pump impellers and casings, and explore the high-dimensional input space using the calibrated WearGP framework. Our approach is similar to Dai et al. [20] in the sense that both utilize GP as a ML-based prediction, where the objectives are similar to Shamshirband et al. [17] and Pandya [18] in terms of predicting wear as global QoIs. However, compared to all previous works, we demonstrate that our approach is highly accurate ($R^2 > 0.99$) as a ML-based wear prediction model.

2 Methodology

In this section, we describe the WearGP methodology, its validation against CFD results in a 3D impeller wear model [3] and a 3D casing wear model [4, 21], which are our previous works. A brief description is provided for the sake of completeness. An Eulerian-Eulerian framework is utilized, and the continuity and momentum equations of the mixture and different solids species are derived using volume and time averaged governing equations. The Spalart-

Allmaras turbulence model [22] and Spalding wall functions are employed, and the set of nonlinear governing equations in the finite element problem are solved iteratively by Newton's method with tuned under-relaxation factors until a given residual level is achieved. The SUPG (Streamwise Upwind Petrov Galerkin) finite element formulation is used, where all systems of algebraic equations are solved using Intel PARDISO solver, which is a OpenMP-based shared memory parallel linear solver. Based on the CFD solutions, the constitutive model for wear prediction is then utilized to predict the total wear as a function of concentration, density, velocity magnitude, tangential velocity, shear stress, impingement angle, and the particle size. The constitutive wear model is calibrated for white iron alloys, which are the most pervasive metal used in slurry pumps [23]. The numerical wear prediction is computed from the CFD solutions and the constitutive model for wear depending on the pump materials. The total wear is considered to be a highly nonlinear function of fluid and solids density, velocity magnitude, tangential velocity, shear stress, solids impingement angle, solids concentration, and the particle size distribution.

2.1 Gaussian process

We adopt the notation from Shahriari et al. [24] and our previous works [25, 26, 27] for the sake of consistency. Assume that f is an unknown smooth function of $\boldsymbol{x}$, where the d-dimensional input is represented as $\boldsymbol{x} \in \mathcal{X}$, where $\mathcal{X}$ is the input space. A $GP(\mu_0, k)$ with the prior mean function $\mu_0(x) : \mathcal{X} \mapsto \mathbb{R}$ and a positive-definite kernel, or covariance function $k : \mathcal{X} \times \mathcal{X} \mapsto \mathbb{R}$ is a nonparametric model over functions f. In the GP formulation, we also assume that $\boldsymbol{f} = f_{1:n}$ is jointly Gaussian, and the observation y is Gaussian given f, i.e.

$$\boldsymbol{f}|\boldsymbol{X} \sim \mathcal{N}(\boldsymbol{m},\ \boldsymbol{K}) \tag{1}$$

$$\boldsymbol{y}|\boldsymbol{f}, \sigma^2 \sim \mathcal{N}(\boldsymbol{f},\ \sigma^2\boldsymbol{I}) \tag{2}$$

where $m_i := \mu(\boldsymbol{x}_i)$, and $K_{i,j} := k(\boldsymbol{x}_i,\ \boldsymbol{x}_j)$. The prior distribution induced by the GP is described in Equation 1.

The covariance kernel k describes the general behavior of the unknown function f. Stationary kernels, which are shift invariant, are typically used. One of the most common kernels is the squared exponential kernel, which is a special case of a Matérn kernel as $\nu \to \infty$. This kernel can be described mathematically as

$$\boldsymbol{K}_{i,j} = k(\boldsymbol{x}_i, \boldsymbol{x}_j) = \theta_0^2 \exp\left(-\frac{r^2}{2}\right), \tag{3}$$

where $r^2 = (\boldsymbol{x} - \boldsymbol{x}')\boldsymbol{\Gamma}(\boldsymbol{x} - \boldsymbol{x}')$, and $\boldsymbol{\Gamma}$ is a diagonal matrix of d squared length scale θ_i. The hyper-parameters θ of the GP are determined by maximizing the likelihood function, where the log marginal likelihood is described as

$$\begin{aligned} \log p(\boldsymbol{y}|\boldsymbol{x}_{1:n}, \theta) = &-\frac{1}{2}(\boldsymbol{y} - \boldsymbol{m}_\theta^T)(\boldsymbol{K}^\theta + \sigma^2\boldsymbol{I})^{-1}(\boldsymbol{y} - \boldsymbol{m}_\theta) \\ &- \frac{1}{2}\log|\boldsymbol{K}^\theta + \sigma^2\boldsymbol{I}| - \frac{n}{2}\log(2\pi), \end{aligned} \tag{4}$$

where $\boldsymbol{m}_\theta(\boldsymbol{x})$ denotes the global trend of the GP, and σ^2 is the intrinsic variance of observations. Hooke and Jeeves's method [28], which is a derivative-free direct search method, is used to maximize the likelihood function. As Equation 4 involves computing the inverse of the covariance matrix of size $n \times n$ where n is the number of training data points, the algorithmic complexity of the training procedure for GP is $O(n^3)$.

The posterior Gaussian distribution, given the prior in Equation 1, can be fully characterized by the posterior mean and posterior variance functions, respectively, as

$$\mu_n(\boldsymbol{x}) = \mu_0(\boldsymbol{x}) + \boldsymbol{k}(\boldsymbol{x})^T(\boldsymbol{K} + \sigma^2\boldsymbol{I})^{-1}(\boldsymbol{y} - \boldsymbol{m}), \tag{5}$$

and

$$\sigma_n^2 = k(\boldsymbol{x},\ x) - \boldsymbol{k}(\boldsymbol{x})^T(\boldsymbol{K} + \sigma^2\boldsymbol{I})^{-1}\boldsymbol{k}(\boldsymbol{x}), \tag{6}$$

Here, $\boldsymbol{k}(\boldsymbol{x})$ is the covariance vector between the test point $\boldsymbol{x}$ and the training data points $\boldsymbol{x}_{1:n}$. Compared to other ML approaches, Guassian processes suffer from a scalability issue, but perform well in a small data regime, unlike most ML approaches. GP formulation also enables UQ for prediction, which is rare to see in ML methods. This means that results are described with error margins, which is highly desirable for wear modeling.

2.2 WearGP framework

Figure 1 compares the process of creating wear predictions between a conventional CFD approach and a machine learning approach. The inputs $\boldsymbol{x} = (\boldsymbol{x}_{\text{solids}},\ \boldsymbol{x}_{\text{liquids}},\ \boldsymbol{x}_{\text{BCs}},\ \boldsymbol{x}_{\text{materials}})$ are parameterized into several categories to model wear as a result of complex interactions between the carrier fluid, the solids/particles, and the pump materials. $\boldsymbol{x}_{\text{solids}}$ represents solids particle properties, including particle size distribution, concentration by volume, hardness, sphericity, and shape factor. $\boldsymbol{x}_{\text{liquids}}$ represents the carrier fluid properties, including density, viscosity, and temperature. $\boldsymbol{x}_{\text{BCs}}$ represents the boundary conditions of the CFD simulations, which is an indirect result of the operating conditions. For example, the inlet velocity is a function of head and flow rate of the pump. $\boldsymbol{x}_{\text{materials}}$ describes the constitutive wear behavior of the pump materials under different conditions, such as local solids concentration, solids impact angle, solids velocity, wall shear stress, and velocity and pressure fields.

Wear response of the pump components, denoted as $\dot{W}$,

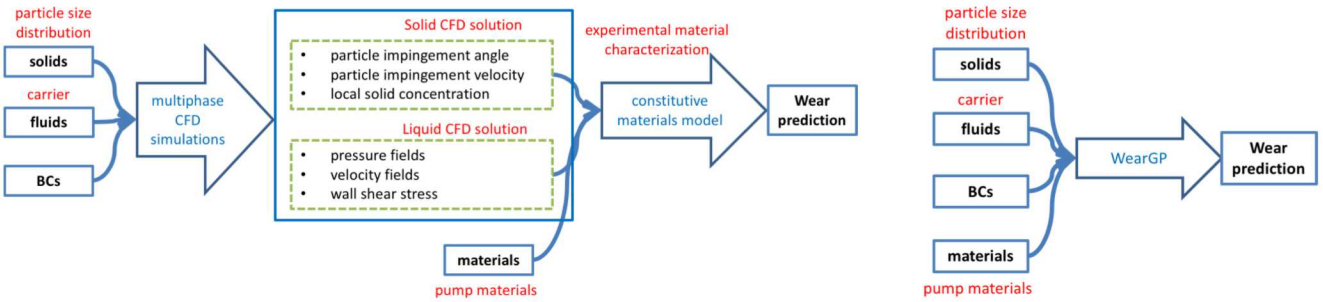

(a) Conventional CFD wear prediction.

(b) WearGP framework.

Fig. 1: Comparison of conventional and machine learning approaches for wear prediction.

is a function of $(\boldsymbol{x}_{\text{solids}}, \boldsymbol{x}_{\text{fluid}}, \boldsymbol{x}_{\text{BCs}}, \boldsymbol{x}_{\text{materials}})$, i.e.

$$\dot{W} = \dot{W}(\boldsymbol{x}_{\text{solids}}, \boldsymbol{x}_{\text{fluid}}, \boldsymbol{x}_{\text{BCs}}, \boldsymbol{x}_{\text{materials}}). \tag{7}$$

The conventional workflow in Figure 1a can be considered as a directed graph, where the inputs $(\boldsymbol{x}_{\text{solids}}, \boldsymbol{x}_{\text{fluid}}, \boldsymbol{x}_{\text{BCs}}, \boldsymbol{x}_{\text{materials}})$ are the sources and the wear prediction output is the sink. The WearGP framework shortcuts the conventional CFD approach in wear prediction by constructing a black-box function directly from the inputs to the output (Figure 1b), assuming that there is sufficient data. The wear dataset can be conveniently generated using a high-performance computing (HPC) platform by sampling CFD simulations with different input parameters.

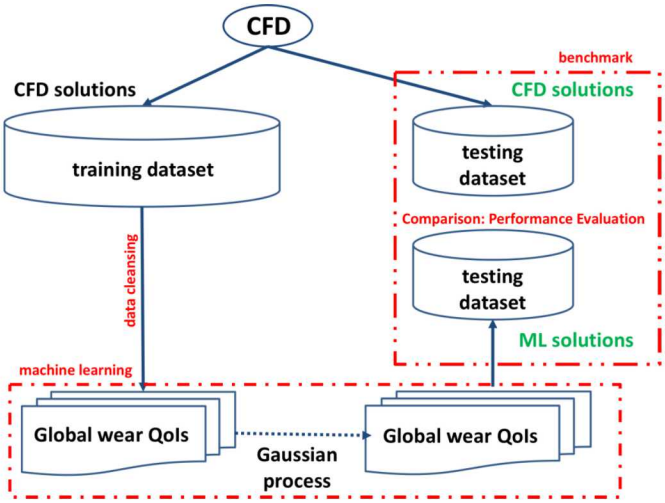

Fig. 2: Workflow of WearGP framework for a specific pump component to predict global wear QoIs.

Figure 2 presents the overall WearGP workflow as a supervised machine learning approach to predict the wear as global QoIs. A wear dataset is generated, then split into the training and testing datasets. For each global wear QoI, a GP is constructed based on the training dataset. Next, the WearGP prediction is compared against the CFD wear prediction for validation purposes.

3 Validation of the WearGP framework

We use a single pump assembly, which is GIW pump impeller 0509X LSA-36 5525D 7671D-A1, as a case study to demonstrate the applicability of the WearGP framework to predict wear as global QoIs. In this case study, 144 simulations are used as a training dataset, whereas 40 simulations are used as a testing dataset. The training dataset, including 144 training data points, are sampled from head $H \in \{35,\ 50,\ 65\}$m, percentage of best efficient point flow rate $\%BEPQ \in \{0.70,\ 1.00,\ 1.30\}$, median particle size $d_{50} \in \{150,\ 300,\ 450\}$ μm, and concentration by volume $C_v \in \{0.10,\ 0.20,\ 0.30,\ 0.40\}$. The corresponding flow rate Q is then solved for using an in-house program, given these operating conditions. The testing dataset includes 40 data points, where each point corresponds to uniformly random operating conditions between the lower and upper bounds of the training dataset. Interested readers are referred to our previous work for the full description of training and testing datasets (Tables 1 and 2 in [1]). The set of operating conditions $\{H,\ Q,\ d_{50},\ C_v\}$ constitutes the input for the WearGP framework, where the wear rates $\dot{W}$'s are considered its outputs.

It is important to point out that the WearGP approach is capable of producing the whole CFD solutions, i.e. the nodal CFD wear predictions. However, as the number of trained GPs must equal to the number of nodes, the training time increases significantly. To demonstrate the capability of the WearGP framework, the CFD solutions, where detailed descriptions are summarized in Section 2 and previous works [3,4,21], are compared against the ML predictions by the WearGP approach. In Section 3.1, the CFD solutions are compared with the local WearGP predictions, whereas in Section 3.2, the CFD solutions are compared with the global WearGP predictions.

3.1 Validation of WearGP framework on local wear QoIs

In this section, we show some results from our previous work [1] to demonstrate that the WearGP framework is capable of predicting wear as local wear QoIs for both our

impeller and casing wear models.

Figure 3 shows the comparison between CFD wear results and the WearGP results for the 3D impeller wear model on the impeller shroud, hub, pressure, and suction surfaces, respectively, where excellent comparison is observed. Figure 4 shows the comparison between the CFD and WearGP wear predictions for the 3D casing wear model, where similar wear patterns are observed. The wear predictions agree very well, both qualitatively and quantitatively, in predicting wear hot spot near the tongue of the pump casing.

3.2 Validation of WearGP framework on global wear QoIs

In this section, the WearGP framework is utilized to predict the global wear QoIs. For the 3D impeller model, the global wear QoIs are the average and the maximum wear rate on four different surfaces of the impeller: shroud, hub, pressure and suction sides of the impeller vane. For the 3D casing model, the global wear QoIs are the average and the maximum wear rate in the mid-plane of the pump casing.

Figure 5a to Figure 5d show the correlation and quantitative comparison between the CFD wear results and the WearGP prediction on shroud and hub surfaces for both average and max wear QoIs. The correlation is slightly stronger for average wear QoIs compared to max wear QoIs. Particularly, for shroud surface, R^2 correlation coefficient is only 0.9324 for the max wear QoI, but increases to 0.9990 for average wear QoI, possibly due to the sensitivity of the max wear QoI in the CFD simulation.

Figure 5e to Figure 5h show the correlation and quantitative comparison between the CFD wear results and the WearGP prediction on pressure and suction sides of the impeller vane. For the pressure side of the vane, a smaller wear rate is observed, and the prediction error is higher, compared to the suction of the vane. The average wear QoI did not increase the prediction accuracy on the pressure side of the vane, possibly due to the small wear rate. On the suction side, the CFD wear results and the WearGP results agree very well with $R^2 > 0.99$.

Figure 5i shows the correlation and quantitative comparison of the average wear QoI along the impeller vane, on both the pressure and suction sides, with $R^2 > 0.99$. Because this QoI is one of the most influential factors to predict the remaining life of an impeller in industrial settings, it will be used as a representative QoI to study the effects of operating conditions on the impeller wear rate.

Figure 6a and Figure 6b show the correlation and quantitative comparisons between the CFD wear results and the WearGP prediction on the mid-plane of the pump casing ($z = 0$), in terms of both average and max wear QoIs. Typically, there are two places for the pump casing to reach its maximum wear rate. The first place is the tongue of the casing, because this location experiences the maximum impact wear. The second place is the 6 o'clock location of the pump casing, because this location is exposed to the maximum sliding wear since the solids particles attain their maximum velocity due to centrifugal force. The maximum wear QoI is

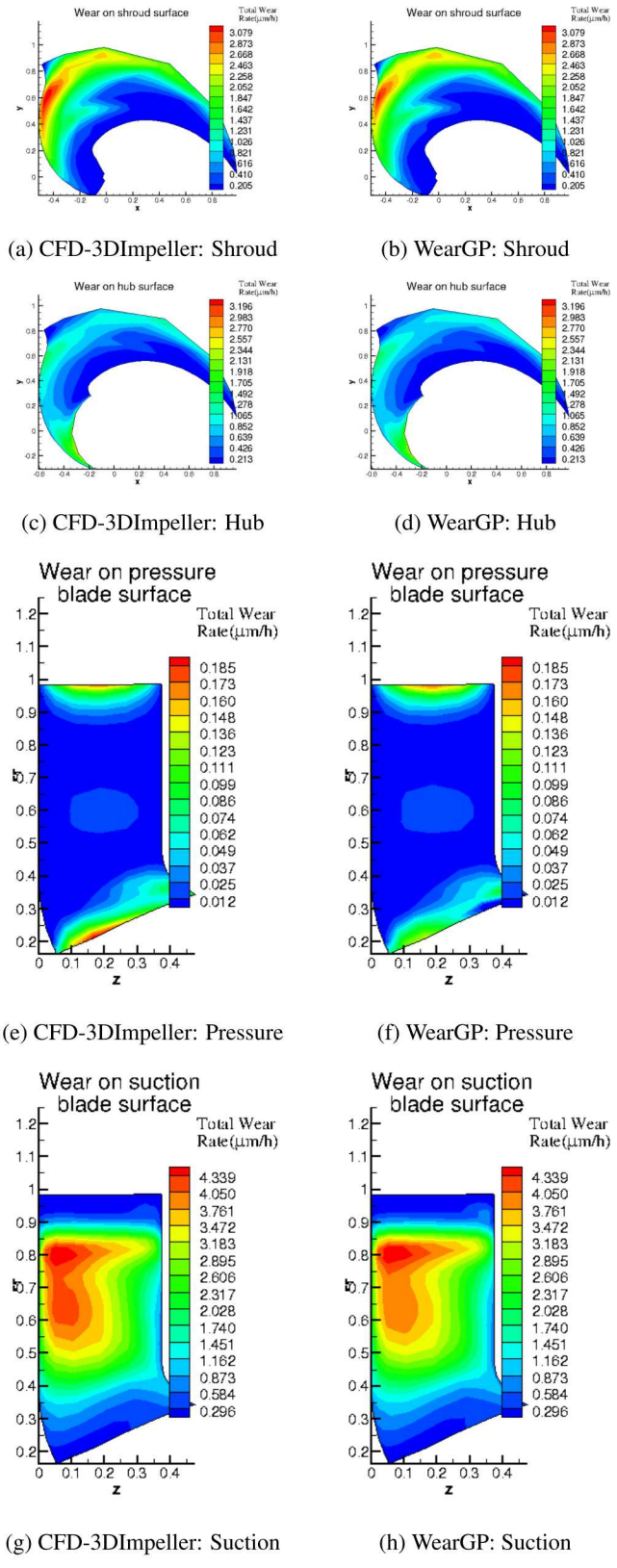

(a) CFD-3DImpeller: Shroud (b) WearGP: Shroud

(c) CFD-3DImpeller: Hub (d) WearGP: Hub

(e) CFD-3DImpeller: Pressure (f) WearGP: Pressure

(g) CFD-3DImpeller: Suction (h) WearGP: Suction

Fig. 3: Comparison of 3D impeller CFD and WearGP predictions in test case #5.

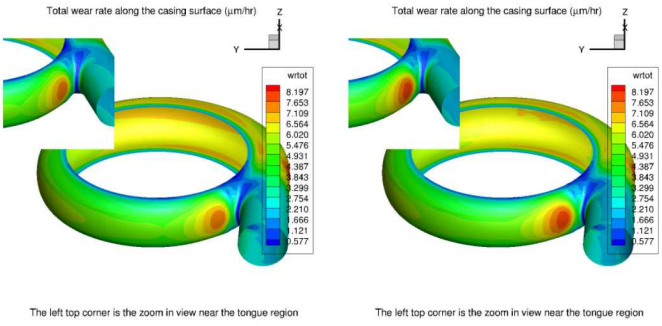

(a) CFD. (b) WearGP.

Fig. 4: Comparison of 3D casing CFD and WearGP predictions in test case #5.

captured with $R^2 \approx 0.98$, whereas the average wear QoI is captured with $R^2 > 0.99$, indicating that the WearGP framework is highly predictive.

To quantify the uncertainty associated with the GP prediction, the error bar of one standard deviation (i.e. $\mu \pm 1.0\sigma$) is provided in Figures 5 and 6. As expected, the maximum wear rates are associated with more noise compared to the average wear rates on all surfaces of the impeller, as well as the casing. The error bars are relatively large because only a small amount of data is used to train the WearGP model. It is expected that the error bar would reduce as the amount of training data increases. The posterior mean is however fairly accurate with $R^2 > 0.95$ when the WearGP prediction results are compared with the CFD results.

4 Effects of operating conditions on wear performance

In Section 3, we have demonstrated that the WearGP framework is capable of predicting wear QoIs accurately with $R^2 > 0.99$ for most QoIs. In this section, we use the calibrated WearGP to explore the effects of varying the operating conditions $\{H,\ Q,\ d_{50},\ C_v\}$ by interpolation. The average wear QoI of the pressure and suction sides in Figure 5i is used for the 3D impeller wear model, and and the average wear QoI in the mid-plane in Figure 6a is used for the 3D casing wear model. It is noteworthy to point out that both of these QoIs have been calibrated with high accuracy ($R^2 > 0.99$), demonstrating that the WearGP framework is reliable.

4.1 3D impeller

Figure 7a and Figure 7b show the behavior of the average wear QoIs from the 3D impeller wear model in Figure 5i at fixed $\{H,\ Q\}$ and fixed $\{d_{50},\ C_v\}$, respectively.

In Figure 7a, the parameters are set as $d_{50} = 300\mu$m and $C_v = 0.20$, where the head and flow rate vary in $H \in [35,\ 65]$m, $Q \in [6000,\ 12000]$ GPM. In Figure 7b, the parameters are set as $H = 50$m and $Q = 10{,}000$ GPM, where the median particle size and concentration vary as $d_{50} \in [150,\ 600]\mu$m, $C_v \in [0.10,\ 0.40]$.

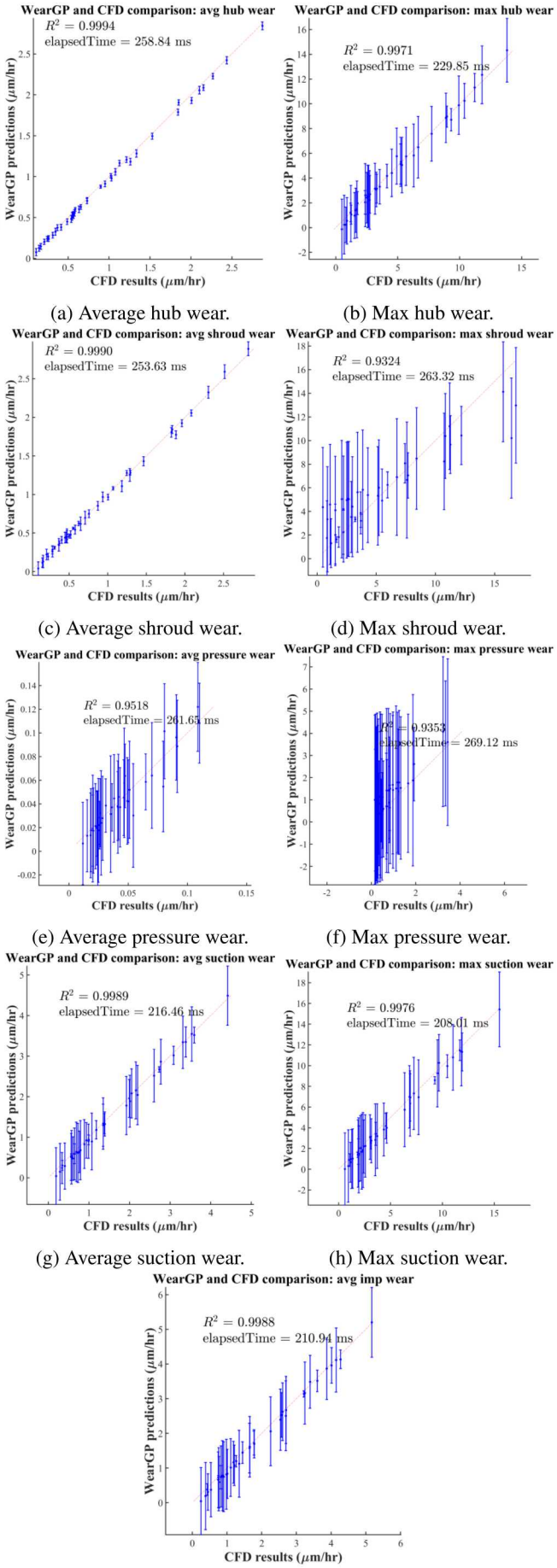

(a) Average hub wear. (b) Max hub wear.

(c) Average shroud wear. (d) Max shroud wear.

(e) Average pressure wear. (f) Max pressure wear.

(g) Average suction wear. (h) Max suction wear.

(i) Average impeller vane wear.

Fig. 5: Validation of WearGP on global wear QoIs on impeller shroud, hub, pressure and suction surfaces, and average wear on both surfaces along the impeller vane.

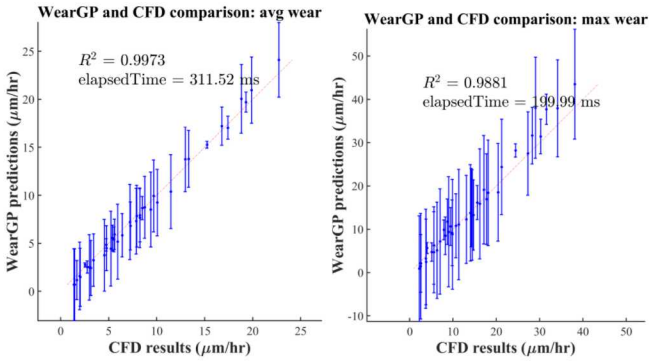

(a) Average casing wear. (b) Max casing wear.

Fig. 6: Validation of WearGP on global wear QoIs on casing wear at mid-plane $z = 0$.

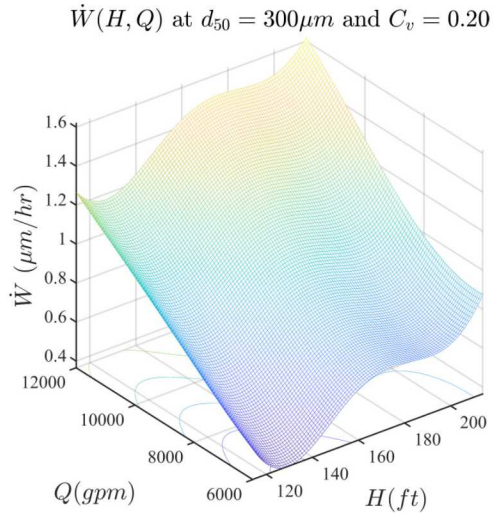

(a) Effects of H and Q on wear.

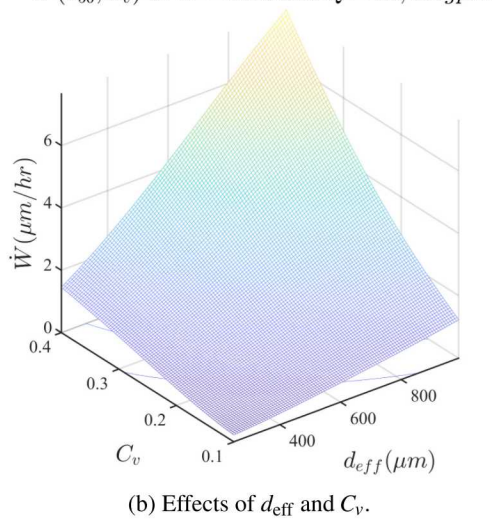

(b) Effects of d_{eff} and C_v.

Fig. 7: Effects of operating conditions on 3D impeller wear

In Figure 7a, the average wear QoI is a non-linear function of H and Q, where multiple local minima are observed. This implies that for a fixed flow rate Q, there might be an optimal H corresponding to the optimal wear rate $\dot{W}$. The average wear rate QoI generally increases with respect to both increasing Q and increasing H, even though the behavior in H is more complicated. However, the flow rate Q seems to have a dominant effect on the increase of the wear rate QoI, compared to the effect of the head H. In Figure 7b, the average wear rate QoI is a monotonic function of both C_v and d_{50}. An increase in either d_{50} and C_v lead to an increase in the average wear rate QoI. The effect of d_{50} is more severe at high concentration C_v (e.g. $C_v = 0.40$), compared to at low concentration C_v (e.g. $C_v = 0.10$). For fine-grain particle size distribution ($d_{50} \approx 150\mu$m), a significant increase in concentration by volume C_v does not dramatically increase the wear rate. The combination effect of d_{50} and C_v is severe in terms of wear rate.

4.2 3D casing

Figure 8a and Figure 8b shows the behaviors of the average wear QoI from the 3D casing wear model in Figure 6a at fixed $\{H, Q\}$ and fixed $\{d_{50}, C_v\}$, respectively.

In Figure 8a, the parameters are set as $d_{50} = 300\mu$m and $C_v = 0.20$, where the head and flow rate vary as $H \in [35,\ 65]$ m, $Q \in [6000,\ 12000]$ GPM. In Figure 8b, the parameters are set as $H = 50$ m and $Q = 10{,}000$ GPM, where the median particle size and concentration vary as $d_{50} \in [150,\ 600]\mu$m, $C_v \in [0.10,\ 0.40]$.

In Figure 8a, the average wear QoI is a non-linear function of H and Q. At very low head, the average wear rate QoI also increases. In the 3D casing wear model, the average wear rate QoI increases with respect to both increasing Q and increasing H, but is dominated by the head H more than the flow rate Q, whereas Q dominated more than H in the 3D impeller wear model. In Figure 8b, the average wear rate QoI is a monotonic function of both C_v and d_{50}, similar to the 3D impeller wear model.

An increase in either d_{50} or C_v leads to an increase in the average wear rate QoI. The effect of d_{50} is more severe at high concentrations (e.g. $C_v = 0.40$), compared to low concentrations (e.g. $C_v = 0.10$). For fine-grain particle size distributions ($d_{50} \approx 150\mu$m), a significant increase in concentration by volume C_v does not dramatically increase the wear rate. The combined effect of $\{d_{50},\ C_v\}$ is severe in terms of the wear rate. In the 3D casing wear model, the median particle size d_{50} has a greater effect on the average wear rate QoI (Figure 8b) than it does in the 3D impeller wear model (Figure 7b).

For the 3D impeller CFD wear models, the maximum wear rate and its corresponding location often vary with respect to operating conditions. In some cases, the model has been shown to be predictive for pump cavitation, which creates collapsing bubbles that is locally detrimental to the pump impeller. The local wear results by the 3D impeller CFD wear model provide such computational insights for relevant personnels, where the WearGP further enhances its capability into real-time predictions. For the 3D casing CFD wear models, the maximum wear rate location often occurs either at 6 o'clock location or at the pump casing tongue,

where the former location corresponds the maximum sliding wear rate and the later location corresponds to the maximum impact wear rate. The computational results provided by the 3D casing CFD wear model match qualitatively and quantitatively engineering intuition. It is possible that the interaction between particles scales as $O(n^2)$, where n is the number of particles, and this effect has a more severe implication when the particles are substantially large.

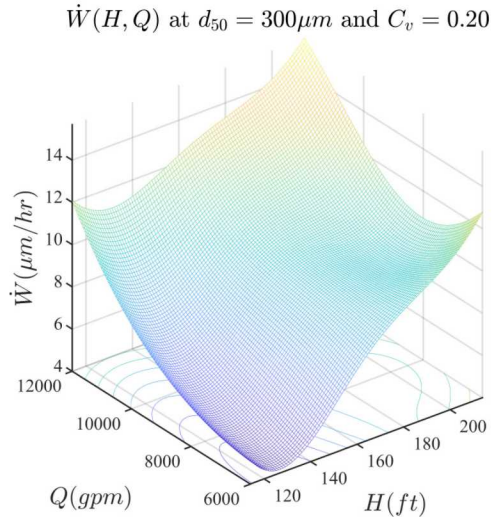

(a) Effects of H and Q on wear.

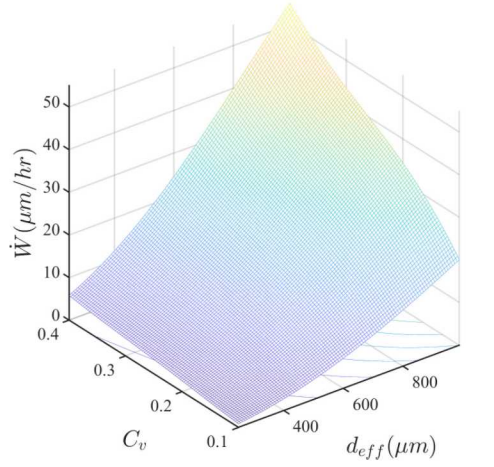

(b) Effects of d_{eff} and C_v.

Fig. 8: Effects of operating conditions on 3D casing wear

5 Discussion

In this paper, we employed a Gaussian process surrogate model to predict the wear rates of pump impellers and casings as global QoIs, where the inputs are the operating conditions. There are several important advantages of GP modeling, compared to other machine learning methods. First, GP is very competitive for small data regimes, and it has been shown that GP behaves similarly to a single layer of neural network with infinite nodes [29, 30]. Second, GP is one of the few ML techniques that enables UQ for prediction. The UQ feature is particularly useful for engineering reliability purposes. Last but not least, GP can also be used as an active learning approach for design optimization, which makes it applicable for impeller and casing design problems. For example, a mixed-integer Bayesian optimization (BO) method [31] can be deployed to optimize the impeller design, where the number of vanes is a discrete parameter. Furthermore, the parallel BO extension can be deployed on a HPC platform to derive the optimal design in a far shorter time [32, 33], and a multi-objective BO framework [34] could be utilized to optimize multi-objectives, such as hydraulic efficiency and wear rates. A multi-fidelity BO framework [35, 36] can be utilized to couple computational and experimental wear data.

It was previously known that an increase in d_{50} would increase the wear rate. The effects of the particle size distribution have been studied [37], where the effective particle size diameter, d_{eff}, is determined to be $d_{\text{eff}} = 1.65 d_{50}$, where d_{50} is the median particle diameter in the particle size distribution. However, in this paper, we show for the first time that the effects of concentration by volume C_v and the particle size distribution d_{50} are non-linear, in the sense that the combined effects yield much higher wear rates than the sum of each individual factor.

While the effects of C_v and d_{50} are similar in both 3D impeller and 3D casing wear models, the effects of the head H and volumetric flow rate Q are quantitatively different. In the 3D impeller wear model, the flow rate Q seems to be dominant, whereas in the 3D casing wear model, the head H seems to play a larger role in wear increase.

In this case study, only one casing and one impeller are considered. However, in practice, as the impeller and casing designs vary, it may be important to generalize the WearGP framework such that pump design features can be included in the wear rate prediction. Such an inclusive ML approach may enable design engineers to search for the optimal design subject to the known pump operating conditions, through minimizing the overall wear rate by tuning the design parameters.

The usage of Spalart-Allmaras, which is a one-equation turbulence model, for pumps is not uncommon; for example, Baoling [38] utilized the Spalart-Allmaras turbulence to model low-specific-speed centrifugal impellers and pointed out the advantage of using the one-equation turblence model to simulate the flow field in impellers channels: compared to two-equation model, Spalart-Allmaras is more numerically stable and requires less amount of computation, while compared to zero-equation model, the turbulent eddy viscosity field is always continuous [38]. Mao et al. [39] also compared various turbulence models and concluded that SST seems superior compared to $k-\varepsilon$, RNG $k-\varepsilon$, and $k-\omega$. However, we acknowledge the limitations of the Spalart-Allmaras turbulence model for centrifugal pumps, and the issue would be addressed in future work. Even though the choice of turbulence models is relatively comparable, ultimately they also contain numerical approximation errors, and thus do not always capture experimental measurements.

To this end, numerous studies have been performed to capture model-form uncertainties for RANS with different turbulence models, including [40] and [41]. The Spalding wall function is used as a boundary condition to provide a turbulent kinematic viscosity condition that gives a continuous profile to the wall ($y^+ = 0$), in order to match both the viscous and inertial sublayers.

It is noteworthy to point out that the UQ enabled by GP in this study is not accounted for the CFD UQ, which is an active research area in the CFD community. Of particular interests is the model-form UQ for different turbulence models and RANS simulations. It is also important to note that only a few ML frameworks can afford data-driven UQ feature, where GP is one of those. In this study, the UQ feature of the proposed WearGP framework is highlighted for both CFD impeller and casing wear models in centrifugal slurry pumps.

From a data analytic point of view, linear and non-linear dimension reduction methods, for example, active subspace [42] and variational auto-encoder [43], have been utilized to reduce the dimensionality of inputs. From a hydraulic engineering point of view, the operating conditions of a pump are solely determined by the intersection of the system curve and the pump curve. Thus, the head H and the flow rate Q are chosen on this basis for a fixed pump. A comparison study has been conducted in [1], where the basis of (H, Q, d_{50}, C_v) is shown to outperform another choice.

The training time for WearGP for global QoIs is computationally cheap, i.e. less than 1s with no parallelization, not including the amount of time used to generate the training and testing datasets. The testing time for the CFD approach is 1,061,203 s [1], whereas the WearGP approach for global QoIs is around 200 ms. The speedup factor is estimated roughly about $0.5 \cdot 10^7$x, which is a significant improvement for using UQ/ML approaches.

Indeed, one of the advantages of the proposed WearGP framework is the fusion between experimental and computational data. Typically, comparison between computational and experimental data is often performed to draw conclusion and determine which model is best in terms of predictive capability. Yet, there is a lack of research effort in fusing experimental and computational data together, which can easily outperforms computational predictions alone, if the objective is to reproduce experimental data. Thus, even the best computational model is inferior to any data-driven approach that considers both types of data. One possible way is to employ a multi-fidelity framework and consider computational data as low-fidelity and experimental data as high-fidelity. By exploiting the correlation between low- and high-fidelity data [35, 36], a better prediction resembling experiments can be achieved. This direction is currently active and remains as further research. The WearGP framework is demonstrated using 3D CFD casing and 3D CFD impeller model for one pump with various operation conditions. Since the case of pump geometry is randomly selected, we expected that the proposed WearGP framework would hold for other similar pump geometries, even with different sizes. For interested readers, numerical verification and experimental validation studies can be found in our previous studies [1, 3, 4, 21].

Compared to our previous work [2] where one-factor-at-a-time approach was employed, the WearGP framework is much more efficient in capturing the nonlinear behavior of the wear rate in different components [44]. The nonlinear behavior is particularly severe with the particles, as the wear is sensitive to the combination of the concentration by volume and the median particle diameter. It is well-known that the characterization of particles is a challenging and sophisticated problem, as the particles are many different sizes. As a result, statistical descriptors are needed to describe a population of particles. For non-spherical particles, roundness and sphericity are also used to describe particles. The most common choice is the effective roundness and sphericity, which are equivalent to the mean (i.e. first statistical moment) with respect to the particle distribution. Uncertainty quantification of wear, both computationally and experimentally, with respect to the particle distribution remains an opening and challenging topic for future research.

6 Conclusion

In this paper, we applied the WearGP framework to accurately predict wear rates as global wear QoIs and explored the effects of operating conditions on the wear rate of a slurry pump casing and impeller. The WearGP framework has been calibrated with high confidence, where the correlation coefficient $R^2 > 0.99$ for the two wear QoIs in the impeller and casing wear models. The behavior of the average wear rate QoIs are qualitatively similar for both casing and impeller wear models. Generally, the wear rate $\dot{W}$ increases monotonically with increasing head H, increasing median particle size d_{50}, and increasing concentration by volume C_v. Moreover, it has been shown that increasing both d_{50} and C_v results in a significant increase in the wear rate.

Acknowledgements

This research was partially supported by the U.S. Department of Energy, Office of Science, Early Career Research Program, under award 17020246. The views expressed in the article do not necessarily represent the views of the U.S. Department of Energy or the United States Government. Sandia National Laboratories is a multimission laboratory managed and operated by National Technology and Engineering Solutions of Sandia, LLC., a wholly owned subsidiary of Honeywell International, Inc., for the U.S. Department of Energy's National Nuclear Security Administration under contract DE-NA-0003525.

References

[1] Tran, A., Furlan, J. M., Pagalthivarthi, K. V., Visintainer, R. J., Wildey, T., and Wang, Y., 2019. "WearGP: A computationally efficient machine learning framework for local erosive wear predictions via nodal Gaussian processes". *Wear,* **422**, pp. 9–26.

[2] Sellgren, A., Addie, G., Visintainer, R., and Pagalthivarthi, K., 2005. "Prediction of slurry pump component wear and cost". In Annual Texas A&M Dredging Seminar: 19/06/2005-22/06/2005, Western Dredging Association.

[3] Pagalthivarthi, K. V., Furlan, J. M., and Visintainer, R. J., 2013. "Wear rate prediction in multi-size particulate flow through impellers". In ASME 2013 Fluids Engineering Division Summer Meeting, American Society of Mechanical Engineers.

[4] Pagalthivarthi, K. V., and Visintainer, R. J., 2009. "Solid-liquid flow-induced erosion prediction in three-dimensional pump casing". In ASME 2009 Fluids Engineering Division Summer Meeting, American Society of Mechanical Engineers, pp. 611–617.

[5] Pagalthivarthi, K., and Visintainer, R., 2013. "Finite element prediction of multi-size particulate flow through three-dimensional channel: Code validation". *The Journal of Computational Multiphase Flows,* **5**(1), pp. 57–72.

[6] Chang, C.-W., Dinh, N., and Cetiner, S. M., 2017. "Physics-constrained machine learning for two-phase flow simulation using deep learning-based closure relation". In American Nuclear Society Winter Meeting, Washington, DC, pp. 1749–1752.

[7] Zhu, Y., Zabaras, N., Koutsourelakis, P.-S., and Perdikaris, P., 2019. "Physics-constrained deep learning for high-dimensional surrogate modeling and uncertainty quantification without labeled data". *Journal of Computational Physics,* **394**, pp. 56–81.

[8] Liu, D., and Wang, Y., 2019. "Multi-fidelity physics-constrained neural network and its application in materials modeling". *Journal of Mechanical Design*, pp. 1–35.

[9] Wang, J.-X., Wu, J.-L., and Xiao, H., 2017. "Physics-informed machine learning approach for reconstructing Reynolds stress modeling discrepancies based on DNS data". *Physical Review Fluids,* **2**(3), p. 034603.

[10] Wang, J., Wu, J., and Xiao, H., 2017. "A physics-informed machine learning approach of improving RANS predicted reynolds stresses". In 55th AIAA aerospace sciences meeting, p. 1712.

[11] Wu, J.-L., Xiao, H., and Paterson, E., 2018. "Physics-informed machine learning approach for augmenting turbulence models: A comprehensive framework". *Physical Review Fluids,* **3**(7), p. 074602.

[12] Wang, J.-X., Huang, J., Duan, L., and Xiao, H., 2019. "Prediction of Reynolds stresses in high-Mach-number turbulent boundary layers using physics-informed machine learning". *Theoretical and Computational Fluid Dynamics,* **33**(1), pp. 1–19.

[13] Velten, K., Reinicke, R., and Friedrich, K., 2000. "Wear volume prediction with artificial neural networks". *Tribology International,* **33**(10), pp. 731–736.

[14] Zhang, Z., Barkoula, N.-M., Karger-Kocsis, J., and Friedrich, K., 2003. "Artificial neural network predictions on erosive wear of polymers". *Wear,* **255**(1-6), pp. 708–713.

[15] Suresh, A., Harsha, A., and Ghosh, M., 2009. "Solid particle erosion studies on polyphenylene sulfide composites and prediction on erosion data using artificial neural networks". *Wear,* **266**(1-2), pp. 184–193.

[16] Danaher, S., Datta, S., Waddle, I., and Hackney, P., 2004. "Erosion modelling using bayesian regulated artificial neural networks". *Wear,* **256**(9-10), pp. 879–888.

[17] Shamshirband, S., Malvandi, A., Karimipour, A., Goodarzi, M., Afrand, M., Petković, D., Dahari, M., and Mahmoodian, N., 2015. "Performance investigation of micro-and nano-sized particle erosion in a 90 elbow using an ANFIS model". *Powder Technology,* **284**, pp. 336–343.

[18] Pandya, D., Dennis, B., and Russell, R., 2017. "A computational fluid dynamics based artificial neural network model to predict solid particle erosion". *Wear,* **378**, pp. 198–210.

[19] Qu, J., and Zuo, M. J., 2010. "Support vector machine based data processing algorithm for wear degree classification of slurry pump systems". *Measurement,* **43**(6), pp. 781–791.

[20] Dai, W., Cremaschi, S., Subramani, H. J., and Gao, H., 2018. "Uncertainty quantification in erosion predictions using data mining methods". *Wear,* **408**, pp. 108–119.

[21] Pagalthivarthi, K. V., Furlan, J. M., and Visintainer, R. J., 2015. "Finite element prediction of multi-size particulate flow through three-dimensional pump casing". In ASME/JSME/KSME 2015 Joint Fluids Engineering Conference, American Society of Mechanical Engineers, pp. V001T31A002–V001T31A002.

[22] Spalart, P. R., Allmaras, S. R., et al., 1994. "A one equation turbulence model for aerodynamic flows". *Recherche Aerospatiale-French Edition*, pp. 5–5.

[23] Tian, H. H., Addie, G. R., and Pagalthivarthi, K. V., 2005. "Determination of wear coefficients for erosive wear prediction through coriolis wear testing". *Wear,* **259**(1-6), pp. 160–170.

[24] Shahriari, B., Swersky, K., Wang, Z., Adams, R. P., and de Freitas, N., 2016. "Taking the human out of the loop: A review of Bayesian optimization". *Proceedings of the IEEE,* **104**(1), pp. 148–175.

[25] Tran, A., Liu, D., He-Bitoun, L., and Wang, Y., 2020. "Data-driven acceleration of first-principles saddle point and local minimum search based on Gaussian processes". In Uncertainty Quantification in Multiscale Materials Modeling, Elsevier.

[26] Tran, A., He, L., and Wang, Y., 2018. "An efficient first-principles saddle point searching method based on distributed kriging metamodels". *ASCE-ASME Journal of Risk and Uncertainty in Engineering Systems, Part B: Mechanical Engineering,* **4**(1), p. 011006.

[27] Travaglino, S., Murdock, K., Tran, A., Martin, C., Liang, L., Wang, Y., and Sun, W., 2020. "Computational optimization study of transcatheter aortic valve leaflet design using porcine and bovine leaflets". *Journal of Biomechanical Engineering,* **142**.

[28] Hooke, R., and Jeeves, T. A., 1961. ""direct search"solution of numerical and statistical problems". *Journal of the ACM (JACM),* **8**(2), pp. 212–229.

[29] Lee, J., Bahri, Y., Novak, R., Schoenholz, S. S., Pennington, J., and Sohl-Dickstein, J., 2018. "Deep neural networks as Gaussian processes". In ICLR.

[30] Garriga-Alonso, A., Rasmussen, C. E., and Aitchison, L., 2019. "Deep convolutional networks as shallow Gaussian processes". In ICLR.

[31] Tran, A., Tran, M., and Wang, Y., 2019. "Constrained mixed-integer Gaussian mixture Bayesian optimization and its applications in designing fractal and auxetic metamaterials". *Structural and Multidisciplinary Optimization*, pp. 1–24.

[32] Tran, A., Sun, J., Furlan, J. M., Pagalthivarthi, K. V., Visintainer, R. J., and Wang, Y., 2019. "pBO-2GP-3B: A batch parallel known/unknown constrained Bayesian optimization with feasibility classification and its applications in computational fluid dynamics". *Computer Methods in Applied Mechanics and Engineering,* **347**, pp. 827–852.

[33] Tran, A., Scott, M., Furlan, J. M., Pagalthivarthi, K. V., Visintainer, R. J., and Wildey, T., 2019. "aphBO-2GP-3B: A budgeted asynchronously-parallel multi-acquisition for known/unknown constrained Bayesian optimization on high-performing computing architecture". *Reliability Engineering and System Safety*.

[34] Tran, A., Eldred, M., Wang, Y., and McCann, S., 2020. "srMO-BO-3GP: A sequential regularized multi-objective constrained Bayesian optimization for design applications". In Proceedings of the ASME 2020 IDETC/CIE, Vol. Volume 1: 40th Computers and Information in Engineering Conference of *International Design Engineering Technical Conferences and Computers and Information in Engineering Conference*, American Society of Mechanical Engineers.

[35] Tran, A., Wildey, T., and McCann, S., 2019. "sBF-BO-2CoGP: A sequential bi-fidelity constrained Bayesian optimization for design applications". In Proceedings of the ASME 2019 IDETC/CIE, Vol. Volume 1: 39th Computers and Information in Engineering Conference of *International Design Engineering Technical Conferences and Computers and Information in Engineering Conference*, American Society of Mechanical Engineers. V001T02A073.

[36] Tran, A., Wildey, T., and McCann, S., 2020. "sMF-BO-2CoGP: A sequential multi-fidelity constrained Bayesian optimization for design applications". *Journal of Computing and Information Science in Engineering*.

[37] Pagalthivarthi, K. V., Furlan, J. M., and Visintainer, R. J., 2017. "Effective particle size representation for erosion wear in centrifugal pump casings". In ASME 2017 Fluids Engineering Division Summer Meeting, American Society of Mechanical Engineers, pp. V01CT15A004–V01CT15A004.

[38] Baoling, C., Zuchao, Z., Zhang, J., and Ying, C., 2006. "The flow simulation and experimental study of low-specific-speed high-speed complex centrifugal impellers". *Chinese Journal of Chemical Engineering,* **14**(4), pp. 435–441.

[39] Mao, J., Yuan, S., Pei, J., Zhang, J., and Wang, W., 2014. "Applications of different turbulence models in simulations of a large annular volute-type pump with the diffuser". In IOP Conference Series: Earth and Environmental Science, Vol. 22, IOP Publishing, p. 022019.

[40] Xiao, H., Wu, J.-L., Wang, J.-X., Sun, R., and Roy, C., 2016. "Quantifying and reducing model-form uncertainties in Reynolds-averaged Navier–Stokes simulations: A data-driven, physics-informed Bayesian approach". *Journal of Computational Physics,* **324**, pp. 115–136.

[41] Geneva, N., and Zabaras, N., 2019. "Quantifying model form uncertainty in Reynolds-averaged turbulence models with Bayesian deep neural networks". *Journal of Computational Physics,* **383**, pp. 125–147.

[42] Constantine, P. G., Dow, E., and Wang, Q., 2014. "Active subspace methods in theory and practice: applications to kriging surfaces". *SIAM Journal on Scientific Computing,* **36**(4), pp. A1500–A1524.

[43] Diederik, P. K., Welling, M., et al., 2014. "Auto-encoding variational bayes". In Proceedings of the International Conference on Learning Representations (ICLR), Vol. 1.

[44] Chernatynskiy, A., Phillpot, S. R., and LeSar, R., 2013. "Uncertainty quantification in multiscale simulation of materials: A prospective". *Annual Review of Materials Research,* **43**, pp. 157–182.